

The size of the quark-gluon plasma in ultracentral collisions: impact of initial density fluctuations on the average transverse momentum

Fabian Zhou,¹ Giuliano Giacalone,² and Jean-Yves Ollitrault³

¹*Institute for Theoretical Physics, University of Heidelberg, 69120 Heidelberg, Germany*

²*Theoretical Physics Department, CERN, CH-1211 Genève 23, Switzerland*

³*Institut de physique théorique, Université Paris Saclay, CNRS, CEA, F-91191 Gif-sur-Yvette, France*

(Dated: November 7, 2025)

Recent experiments have shown that the mean transverse momentum $\langle p_T \rangle$ of outgoing particles increases as a function of the particle multiplicity in ultracentral nucleus-nucleus collisions at collider energies. This increase was originally predicted on the basis of simulations where the multiplicity increase occurred at constant volume, so that it implied a larger density and temperature. However, recent state-of-the-art simulations have shown that, for some models of initial condition, the volume may vary with the multiplicity in ultracentral collisions. We elucidate this effect by analytically relating the variation of the volume to the radial distribution of the one- and two-point functions of the fluctuating density field. We show that the volume variation is small if the total entropy of the ultracentral collisions scales with the mass number of the colliding isotopes. We argue that probing detailed transverse distributions of initial-state fluctuations through the ultracentral $\langle p_T \rangle$ has nontrivial implications for models of nuclear structure and of the pre-equilibrium stages.

I. INTRODUCTION

Ultracentral Pb+Pb collisions at the Large Hadron Collider (LHC), typically defined as the 0.2% fraction producing the largest number of particles [1], open a unique window on the initial stages of the collision [2, 3]. The reason is that they have essentially zero impact parameter [4], so that two different ultracentral collisions differ only by quantum fluctuations [5]. These quantum fluctuations originate in particular from the wavefunctions of colliding nuclei [6, 7]. They are characterized, to leading order, by the two-point function of the initial entropy density field [8]. This two-point function can be related to two-body correlations within the nucleus [9, 10], and this relation paves the way to detailed theoretical predictions [11, 12]. But there are at present few constraints from heavy-ion experiments, if any, on how fluctuations are distributed through the transverse plane. The only existing constraint is on the variance of the total entropy at zero impact parameter, which is inferred from the tail of the multiplicity distribution [13, 14], and corresponds to the integral of the two-point function.

We show that the increase of the mean transverse momentum $\langle p_T \rangle$ as a function of the collision multiplicity, which has recently been observed in ultracentral Pb+Pb collisions at the LHC [15–17], can be used to constrain the spatial dependence of the two-point function. $\langle p_T \rangle$ is proportional to the effective temperature [18] of the quark-gluon plasma which is produced in the collision, while the collision multiplicity is proportional to the entropy. The temperature is related to the entropy density through the equation of state. Therefore, it has been initially argued [19] that the increase of $\langle p_T \rangle$ probes the equation of state, and more specifically, the speed of sound of high-temperature QCD [20–23]. This was based on the assumption that the multiplicity increase occurs at constant volume. This hypothesis has been criticized on

the basis of careful state-of-the-art simulations [24, 25], which have shown that depending on the details of the initial-state model, the quark-gluon plasma may shrink or swell as the multiplicity increases [22].

We study the size of the quark-gluon plasma in ultracentral collisions and its dependence on the model of initial conditions. We start by recalling in Sec. II the motivations behind the default model of initial conditions, which postulates that the entropy density at the beginning of the hydrodynamic evolution is determined, at a given point of the transverse plane, by $s \propto (t_A t_B)^{0.5}$ [26], where t_A and t_B are the thickness functions (nuclear density integrated over longitudinal coordinate) of colliding nuclei at that point. We then describe (Sec. III) Monte Carlo simulations with exponents ν that vary around 0.5 [24, 27]. In Sec. IV, we show that the size of the quark-gluon plasma can increase or decrease as a function of the multiplicity depending on the value of ν , while it remains constant for the default model ($\nu = 0.5$). In Sec. V, we explain these results by explicating the relation between the system size and the two-point function of the initial entropy density. The default model is worked out analytically in appendices, where we prove that it leads to a constant size (App. A) and discuss the effect of the nucleon width on the mean density profile (App. B). In Sec. VI, we finally argue that the increase of $\langle p_T \rangle$ in ultracentral collisions can be used to infer information about local density fluctuations.

II. UNDERSTANDING $s \propto \sqrt{t_A t_B}$

The crucial quantity for phenomenology is the entropy density at the time τ_h when the system thermalizes. It serves as an initial condition for hydrodynamic calculations and determines multiplicities and spectra of outgoing particles. We assume for simplicity that it is invariant under longitudinal boosts [28], and we denote it by $s(\mathbf{x})$,

where \mathbf{x} is the transverse coordinate. We denote by S its integral over the transverse plane, which we loosely refer to as the total entropy:¹

$$S \equiv \int_{\mathbf{x}} s(\mathbf{x}). \quad (1)$$

In phenomenological studies, the total entropy is typically adjusted to match the observed multiplicity, and it is not part of the model itself. The modeling lies in the variation of the entropy density with \mathbf{x} and, more specifically, how it depends on the thickness functions $t_A(\mathbf{x})$ and $t_B(\mathbf{x})$ (which will be defined more precisely in Sec. III) of incoming nuclei.

In this Section, we briefly recall why the scenario $s \propto \sqrt{t_A t_B}$ is preferred, both from the point of view of comparison with experimental data, and from general theoretical considerations.

It has long been known that the multiplicity produced in a heavy-ion collision is proportional to the number of nucleons (more precisely, to the number of quarks) involved in the collision [29, 30]. Models of the initial entropy density have been elaborated which take into account this constraint by imposing that s is homogeneous of degree 1 in t_A and t_B , e.g., $s \propto (t_A^p + t_B^p)^{1/p}$ [26]. Theory to data comparison systematically favors values of p close to 0 for the entropy density [27, 31], corresponding to $s \propto \sqrt{t_A t_B}$. In particular, this value reproduces well the centrality dependence of elliptic flow and of the measured particle yields.²

We now explain how this scenario also naturally arises from general theoretical considerations [40–42]. We follow the timeline of a nucleus-nucleus collision at ultra-relativistic energies, which consists of several successive stages:

- The collision first produces longitudinally extended tubes of chromoelectric and magnetic fields [43], analogous to strings [44, 45]. At very early proper time τ , their energy density $\varepsilon(\mathbf{x}, \tau)$ is independent of τ and proportional to both thickness functions [27, 46]:

$$0^+ < \tau < \tau_g : \varepsilon(\mathbf{x}, \tau) \propto t_A(\mathbf{x})t_B(\mathbf{x}) \quad (2)$$

- Fields decay into gluons at a time τ_g . This time is related to the energy density through dimensional analysis, up to logarithmic corrections [43]: $\tau_g \propto \varepsilon^{-1/4} \propto (t_A t_B)^{-1/4}$.
- τ_g is typically much smaller than the thermalization time τ_h . In a first approximation, one can neglect interactions, and the longitudinal pressure

they generate [47, 48], for $\tau_g < \tau < \tau_h$. During this free-streaming phase [49], the energy per unit rapidity is conserved. Since the volume is proportional to τ [28] (the transverse expansion can be neglected at early times), $\varepsilon(\mathbf{x}, \tau)\tau$ is constant. Evaluating it at $\tau = \tau_g$, we obtain [50]:

$$\tau_g < \tau < \tau_h : \varepsilon(\mathbf{x}, \tau)\tau \propto (t_A(\mathbf{x})t_B(\mathbf{x}))^{3/4}. \quad (3)$$

- Thermalization occurs at a time which is generically of order $\tau_h \propto T^{-1}$ [51], where the temperature T is related to $\varepsilon(\tau_h)$ by the equation of state. By dimensional analysis, $\varepsilon(\tau_h) \propto T^4$ and $\varepsilon(\tau_h)\tau_h \propto T^3$. On the other hand, the entropy density is proportional to T^3 so that $s(\tau_h)\tau_h \propto T^2$, and one finally obtains [52]:

$$\begin{aligned} s(\mathbf{x}, \tau_h)\tau_h &\propto (\varepsilon(\mathbf{x}, \tau_h)\tau_h)^{2/3} \\ &\propto (t_A(\mathbf{x})t_B(\mathbf{x}))^{1/2}. \end{aligned} \quad (4)$$

This shows that the entropy density profile at the beginning of the hydrodynamic evolution³ is proportional to $\sqrt{t_A t_B}$.

The above modeling is oversimplified, and can be refined at every stage. Yet it provides a solid general motivation for choosing $s \propto \sqrt{t_A t_B}$. We now study the consequences of varying this default initial condition.

III. SIMULATING THE INITIAL STATE WITH THE GENERALIZED TRENTO MODEL

We use the popular TRENTO model of initial conditions [26], which we briefly describe. It starts by sampling the positions of participant nucleons independently according to the Monte Carlo Glauber model [54, 55]. This is typically the most important source of initial-state fluctuations. In order to parametrize additional fluctuations, each participant is assigned a random weight. The probability of this weight is a gamma distribution with unit mean and variance $1/\sqrt{k}$, where the choice of k will be specified below.⁴

The transverse density profile of each participant is modeled as a two-dimensional Gaussian of width $w_p = 0.5$ fm [58, 59]. The effect of varying the nucleon width is discussed in Appendix B. The TRENTO model then defines the thickness functions of each nucleus $t_A(\mathbf{x})$ and $t_B(\mathbf{x})$ by summing the weighted density profiles of all

¹ Strictly speaking, $\tau_h S$ is the entropy per unit rapidity.

² For this reason, the same value is also favored when the TRENTO model is used to initialize the energy density at midrapidity [32–39].

³ Entropy conservation further implies that $s(\tau)\tau$ remains constant until the transverse expansion sets in [53]. Therefore, results of the hydrodynamic calculation do not depend strongly on how one chooses τ_h , provided that it is short enough.

⁴ We do not include here fluctuation effects related to the internal structure of the colliding nucleons [56, 57].

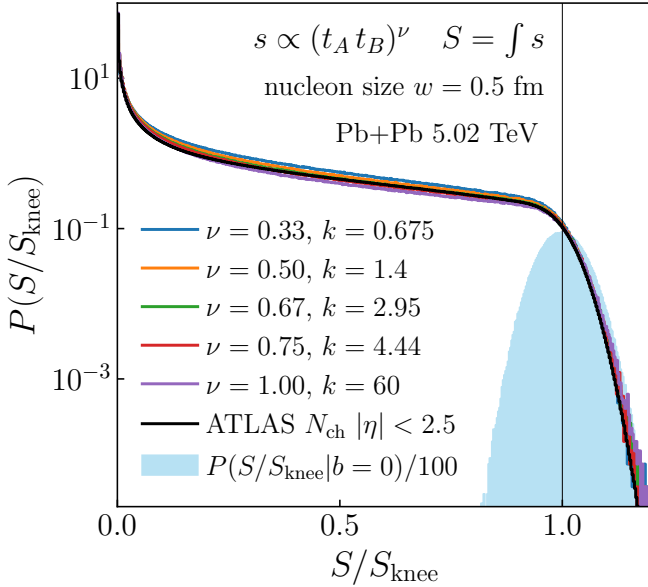


FIG. 1. Histogram of the distribution of the total entropy in a simulation of 10^7 minimum-bias events for various values of ν , rescaled by its average value at $b = 0$, S_{knee} . For each value of ν , the fluctuation parameter k has a different value determined according to Eq. (8). We also plot the distribution of the charged multiplicity measured by ATLAS [16], rescaled in the same way. The shaded area displays the distribution of the total entropy for events with $b = 0$ for $\nu = 0.5$, rescaled by a factor 1/100. It is essentially identical for other values of ν , as a consequence of the constraint (8).

participants (Appendix A). We parametrize the entropy density as

$$s(\mathbf{x}) \propto (t_A(\mathbf{x})t_B(\mathbf{x}))^\nu. \quad (5)$$

The original choice of the TRENTo model is $\nu = 0.5$, which is the prescription advocated in Sec. II. Here, we generalize it by allowing ν to vary [60]. The motivation is that, in most hydrodynamic simulations, the TRENTo model has been used as an initial condition for the *energy* density, rather than entropy density [61]. In order to compensate for this difference, Nijs and van der Schee have generalized the original prescription [27], and parametrized the energy density as⁵

$$\epsilon(\mathbf{x}) \propto (t_A(\mathbf{x})t_B(\mathbf{x}))^{q/2}. \quad (6)$$

At high temperature, the equation of state is approximately conformal, $\epsilon \propto s^{4/3}$, and the correspondence between Eqs. (5) and (6) is

$$q \approx \frac{8}{3}\nu. \quad (7)$$

⁵ More precisely, they define $\epsilon \propto (t_A^p + t_B^p)^{q/p}$, but in practice, p ends up being close to 0, so that we only study the limit $p \rightarrow 0$.

The default value, corresponding to $\nu = 0.5$, is $q = \frac{4}{3}$, but they vary q around this value to study the effect of this parameter in ultracentral collisions [24]. In the same way, we carry out simulations for several values of ν .

We now explain how the fluctuation parameter k of the gamma distribution is chosen. The idea is that the distribution of the total entropy in minimum-bias events should match the multiplicity distribution measured experimentally, up to a global multiplicity factor. This matching is illustrated in Fig. 1 for Pb+Pb collisions at $\sqrt{s_{NN}} = 5.02$ TeV. It is achieved by first simulating events at $b = 0$. We define S_{knee} as the mean value of S for these events, and we rescale the entropy by S_{knee} . The knee of the multiplicity distribution is inferred from data through a Bayesian reconstruction [4]. We then tune the parameter k of the gamma distribution so as to match the tail of the multiplicity distribution. More specifically, we determine k such that the relative variance of the entropy at $b = 0$ is identical to that of the multiplicity, which is also inferred from data [5, 13]:

$$\left(\frac{\sigma_S}{S_{\text{knee}}} \right)^2 \approx 2 \times 10^{-3}, \quad (8)$$

where σ_S denotes the standard deviation of S at $b = 0$. Note that this constraint is not yet enforced in global Bayesian analyses. The values of k satisfying Eq. (8) are displayed in Fig. 1. As ν increases, gamma fluctuations decrease: Fluctuations in nucleon position almost suffice for $\nu = 1$, while strong gamma fluctuations are needed for $\nu = 0.33$ in order to match the tail of the multiplicity distribution.

Fig. 2 illustrates the variation of the density profile with ν for a collision at $b = 0$, where the nucleon positions are the same for all ν . Increasing ν amplifies density contrasts, as expected from Eq. (5). Note, however, that changing ν does not boil down to a nonlinear mapping of the whole profile because of gamma fluctuations, which are sampled independently for each ν .

IV. VARIATION OF SYSTEM SIZE WITH ENTROPY

The main point of this work is to study how the size of the quark-gluon plasma varies with the particle multiplicity or, equivalently, with the total entropy S [62]. We define the rms transverse size R of an event from the initial entropy density profile through [63]

$$R^2 \equiv \frac{1}{S} \int_{\mathbf{x}} |\mathbf{x}|^2 s(\mathbf{x}) - \left| \frac{1}{S} \int_{\mathbf{x}} \mathbf{x} s(\mathbf{x}) \right|^2, \quad (9)$$

where the second term in the right-hand side is a recentering correction, which ensures that R is invariant under translations.

We bin events according to the value of S and evaluate the average value of R^2 , denoted by $\langle R^2 | S \rangle$, in each bin. Results are displayed as dotted lines in Fig. 3, where we

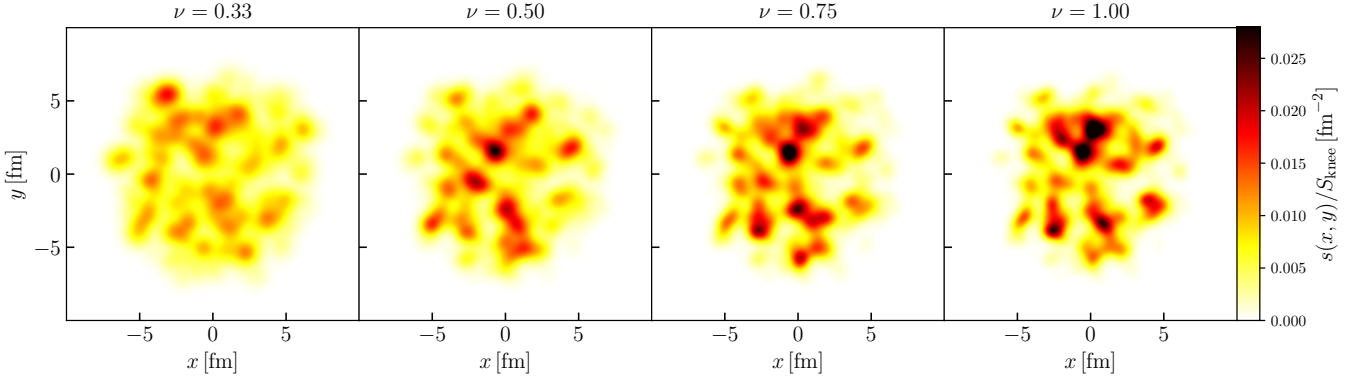


FIG. 2. Entropy density profiles of collisions with $b = 0$, rescaled by a global factor S_{knee} for each ν . We vary ν in Eq. (5), keeping the position of nucleons fixed. The gamma fluctuations normalizing each participant nucleon are however sampled independently for each plot (different k parameters).

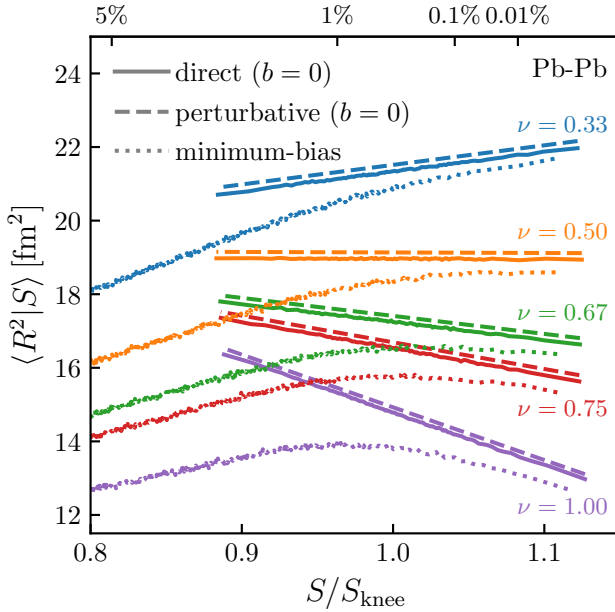


FIG. 3. Variation of the average value of R^2 (Eq. (9)) with the total entropy S (Eq. (1)) in Pb+Pb collisions in the TRENTo model, for various values of the exponent ν in Eq. (5). As in Fig. 1, we rescale S by S_{knee} . Dotted line: minimum-bias events. Solid lines: events with $b = 0$. Dashed lines: perturbative expression for $b = 0$, Eq. (18).

only display values of S/S_{knee} above 0.8, corresponding roughly to the 5% most central collisions. A first observation is that the size decreases as ν increases, as could already be guessed from Fig. 2.

Let us now look at the variation of $\langle R^2|S \rangle$ with S . It first increases, reflecting that the impact parameter decreases and the overlap area between the colliding nuclei increases. Above the knee, the variation depends on the value of ν : The radius keeps increasing for $\nu < 0.5$, while it reaches a maximum and then decreases for $\nu > 0.5$.

This is in qualitative agreement with the *Trajectum* results displayed in Fig. 3 (right) of Ref. [24], which show that the size keeps increasing for $q = 1.05$, corresponding to $\nu \approx 0.39$, and decreases for $q = 1.45$, corresponding to $\nu \approx 0.54$.

In order to understand this behaviour, we carry out a simpler simulation. We fix the impact parameter to $b = 0$, so that the geometry is frozen, and we simulate 5×10^5 events for each ν . The distribution of entropy for these events is a Gaussian centered around the knee [4], as illustrated in Fig. 1. The size of these central events is displayed as solid lines in Fig. 3. Both figures show that minimum-bias results converge asymptotically to $b = 0$ results above the knee. Therefore, in order to understand ultracentral collisions, it suffices to understand the case $b = 0$. Interestingly, for $b = 0$, $\langle R^2|S \rangle$ is essentially constant for the default value, $\nu = 0.5$. This special case is worked out analytically in Appendix A.

V. RELATING THE VARIATION OF THE SIZE TO MICROSCOPIC DENSITY FLUCTUATIONS

Focusing on collisions at $b = 0$, we now relate the variation of the size, R^2 , with S to the statistical properties of density fluctuations.

A. Mean density profile

We first study the mean density profile. We denote by $\kappa_1(\mathbf{x})$ the expectation value of $s(\mathbf{x})$ over all $b = 0$ events. Its integral is the mean value of S at $b = 0$, that is, S_{knee} :

$$\kappa_1(\mathbf{x}) \equiv \langle s(\mathbf{x}) \rangle$$

$$\int_{\mathbf{x}} \kappa_1(\mathbf{x}) = S_{\text{knee}} \quad (10)$$

We choose the origin at the centre of the colliding nuclei. Then, κ_1 depends only on the radial distance $r \equiv |\mathbf{x}|$ by

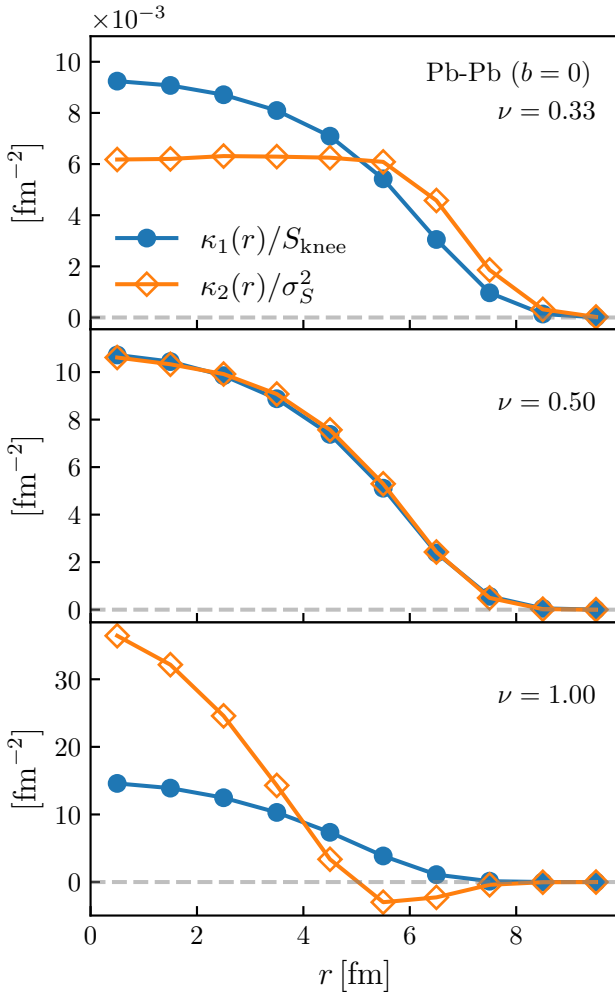


FIG. 4. Variation of the mean entropy density $\kappa_1(r)$ (circles, Eq. (10)) and of the correlation $\kappa_2(r)$ (squares) between entropy density and total entropy (Eq. (14)) for three different values of the exponent ν in Eq. (5). These functions are scaled by S_{knee} and σ_S^2 , respectively, in such a way that they integrate to unity over the transverse plane.

azimuthal symmetry.

Fig. 4 (full symbols) displays $\kappa_1(r)$ for three values of ν , scaled by S_{knee} . The scaled profile depends weakly on ν . The density at the centre $r = 0$ mildly increases as a function of ν , implying a sharper average density distribution.

We denote by R_1 the size of the average profile. It is obtained by replacing $s(\mathbf{x})$ with $\kappa_1(\mathbf{x})$ in Eq. (9), where the last term vanishes by symmetry:

$$R_1^2 \equiv \frac{1}{S_{\text{knee}}} \int_{\mathbf{x}} |\mathbf{x}|^2 \kappa_1(\mathbf{x}). \quad (11)$$

As shown in Fig. 5, R_1^2 decreases as ν increases, in line with the general trend observed in Fig. 3. The decrease of R_1^2 with ν goes along with the increase of the central density $\kappa_1(r = 0)$ in Fig. 4.

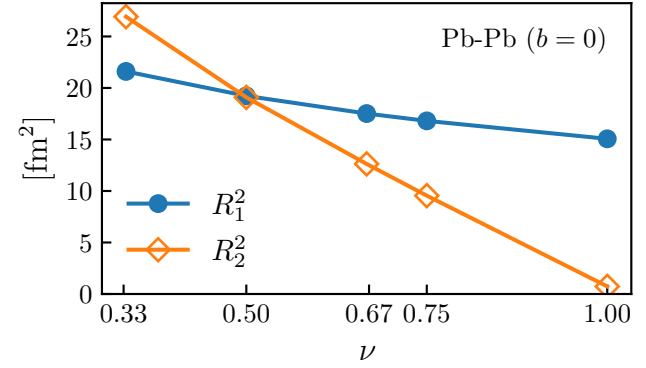


FIG. 5. Variation of R_1^2 and R_2^2 , defined by Eqs. (11) and (17), with the exponent ν in Eq. (5).

B. Fluctuation decomposition

We now carry out a fluctuation decomposition of the entropy density and of the total entropy:

$$s(\mathbf{x}) = \kappa_1(\mathbf{x}) + \delta s(\mathbf{x}) \quad (12)$$

$$S = S_{\text{knee}} + \delta S,$$

where $\delta s(\mathbf{x})$ is the local fluctuation around the mean, and δS its integral over the transverse plane. Inserting the decomposition (12) into Eq. (9) and linearizing in $\delta s(\mathbf{x})$ and δS , one obtains:

$$R^2 = R_1^2 + \frac{1}{S_{\text{knee}}} \int_{\mathbf{x}} |\mathbf{x}|^2 \delta s(\mathbf{x}) - R_1^2 \frac{\delta S}{S_{\text{knee}}}. \quad (13)$$

In order to explain the numerical results in Fig. 3, we must average this expression over events for a fixed total entropy S . For this, we need to evaluate the average $\delta s(\mathbf{x})$ at fixed S , $\langle \delta s(\mathbf{x}) | S \rangle$.

As we shall see shortly, this quantity is determined by the linear correlation between the entropy density $s(\mathbf{x})$ and the total entropy S , which we denote by $\kappa_2(\mathbf{x})$:

$$\kappa_2(\mathbf{x}) \equiv \langle \delta s(\mathbf{x}) \delta S \rangle = \int_{\mathbf{y}} \langle \delta s(\mathbf{x}) \delta s(\mathbf{y}) \rangle. \quad (14)$$

The last equality shows that $\kappa_2(\mathbf{x})$ is the integral of the two point function $\langle \delta s(\mathbf{x}) \delta s(\mathbf{y}) \rangle$, which is the key quantity that defines event-by-event fluctuations [8], over one of the coordinates. If one integrates over the remaining coordinate, one obtains the variance of the total entropy:

$$\int_{\mathbf{x}} \kappa_2(\mathbf{x}) = \langle \delta S^2 \rangle = \sigma_S^2. \quad (15)$$

In order to evaluate $\langle \delta s(\mathbf{x}) | S \rangle$, we assume that fluctuations are approximately Gaussian [64], which is a good approximation for a collision between large nuclei at fixed impact parameter [4, 5]. More specifically, we assume

that the joint distribution of $\delta s(\mathbf{x})$ and δS is a bivariate correlated Gaussian. A simple calculation then gives:

$$\langle \delta s(\mathbf{x}) | S \rangle = \frac{\kappa_2(\mathbf{x})}{\sigma_S^2} \delta S. \quad (16)$$

This equation means that if one fixes the total entropy, there is a shift in entropy density proportional to the excess total entropy δS . Using the normalization (15), one obtains $\int_{\mathbf{x}} \langle \delta s(\mathbf{x}) | S \rangle = \delta S$: The local fluctuation integrates to δS , as it should.

Eq. (16) shows that $\kappa_2(\mathbf{x})$ determines the distribution of the excess density in the transverse plane. Its variation is displayed in Fig. 4 for three values of ν . For $\nu = 0.5$, the distribution of the excess density is exactly the same as that of the mean density, explaining why the radius does not vary (Fig. 3). This result is derived analytically in Appendix A. For $\nu < 0.5$, the excess density is larger near the edge of the fireball, explaining why the radius increases for ultracentral collisions. For $\nu > 0.5$, it is the other way around. Interestingly, the excess density is even *negatively* correlated with the total entropy for large r . The physical mechanism at work in this negative correlation is the fact that the total number of participant cannot exceed the total number of nucleons $2A$.⁶ Because of this conservation law, more participant nucleons near the edge (hence a larger entropy density) implies fewer in the centre. Since most of the entropy is produced in the centre for large ν , this goes along with a decrease in the total entropy, thus explaining the negative correlation.

We define a radius R_2 associated with the function $\kappa_2(\mathbf{x})$ in the same way as R_1 in Eq. (11):

$$R_2^2 \equiv \frac{1}{\sigma_S^2} \int_{\mathbf{x}} |\mathbf{x}|^2 \kappa_2(\mathbf{x}). \quad (17)$$

We keep the same notation for simplicity, but since $\kappa_2(\mathbf{x})$ can be negative, R_2^2 can be negative as well. Its variation with ν is displayed in Fig. 5. It is much steeper than that of the average size R_1^2 .

We are now in a position to explain the Monte Carlo results of Sec. IV. We evaluate the mean value of Eq. (13) at fixed S using Eq. (16). We express the result in terms of R_2 using Eq. (17), and we obtain:

$$\langle R^2 | S \rangle = R_1^2 + (R_2^2 - R_1^2) \frac{\delta S}{S_{\text{knee}}}. \quad (18)$$

The average value of R^2 for $S = S_{\text{knee}}$ is R_1^2 , as one can check by comparing Fig. 3 with Fig. 5. The radius increases or decreases with S depending on whether R_2 is larger or smaller than R_1 . The perturbative result (18) is in excellent agreement with the Monte Carlo calculation, as illustrated in Fig. 3, which is essentially our main result. For $\nu = 0.5$, $R_1 = R_2$ and $\langle R^2 | S \rangle$ is independent of S .

VI. INCREASE OF $\langle p_T \rangle$ IN ULTRACENTRAL COLLISIONS

We now discuss potential experimental implications of our finding. We derive the expression of the increase of the mean p_T of outgoing particles, $\langle p_T \rangle$, in ultracentral collisions, taking into account the possibility that R may depend on the entropy S . Following Ref. [18], we consider that in hydrodynamics $\langle p_T \rangle$ is proportional to an effective temperature T_{eff} . This temperature is a function of the effective entropy density s_{eff} , which is found to be

$$s_{\text{eff}} \approx \frac{S}{1.2\pi(R\sqrt{2})}. \quad (19)$$

The variation of T_{eff} with s_{eff} is determined by the speed of sound c_s at the temperature T_{eff} . By definition of the speed of sound [19],

$$\frac{\delta \langle p_T \rangle}{\langle p_T \rangle} = \frac{\delta T_{\text{eff}}}{T_{\text{eff}}} = c_s^2(T_{\text{eff}}) \frac{\delta s_{\text{eff}}}{s_{\text{eff}}}. \quad (20)$$

Using Eq. (19), one obtains

$$\frac{\delta s_{\text{eff}}}{s_{\text{eff}}} = \frac{\delta S}{S_{\text{knee}}} - \frac{3}{2} \frac{\delta R^2}{R_1^2}, \quad (21)$$

where R_1^2 is the average value of R^2 as shown in Sec. V, and $\delta R^2 = R^2 - R_1^2$ is the variation around the mean. Using Eq. (18), we finally obtain the increase of $\langle p_T \rangle$ as a function of the entropy in collisions at $b = 0$:

$$\frac{\delta \langle p_T \rangle}{\langle p_T \rangle} = c_s^2(T_{\text{eff}}) \left[1 - \frac{3}{2} \left(\frac{R_2^2}{R_1^2} - 1 \right) \right] \frac{\delta S}{S_{\text{knee}}}. \quad (22)$$

We define the slope parameter as

$$\begin{aligned} \text{slope} &\equiv \frac{\delta \ln \langle p_T \rangle}{\delta \ln S} = \frac{\delta \ln \langle p_T \rangle}{\delta \ln N_{\text{ch}}} \\ &= c_s^2(T_{\text{eff}}) \left(1 - \frac{3}{2} \left(\frac{R_2^2}{R_1^2} - 1 \right) \right). \end{aligned} \quad (23)$$

Therefore, the assumption of constant volume originally employed in [20] corresponds to $R_2 = R_1$, and one recovers the result that the slope is $c_s^2(T_{\text{eff}})$. Our formula thus generalizes this case by allowing for a volume variation driven by local density fluctuations and the relative difference between R_2^2 and R_1^2 .

Fig. 6 presents a tentative comparison between *Trajectum* results, obtained from full hydrodynamic simulations, and our results based on Eq. (23). We evaluate the slope in *Trajectum* using results displayed in Fig. 3 (left) of Ref. [24], where we extract the slope of the $\langle p_T \rangle$ curve from the largest values of N_{ch} , corresponding to ultracentral collisions. The increase of the slope as a function of q in *Trajectum* calculations is similar to the increase as a function of ν in our initial-state simulations. More quantitative comparisons with a precise matching between initial conditions and final observables are left for future work.

⁶ This condition is also responsible for the “binomial suppression” of fluctuations of the net baryon number [65–68] and of the charged multiplicity [69].

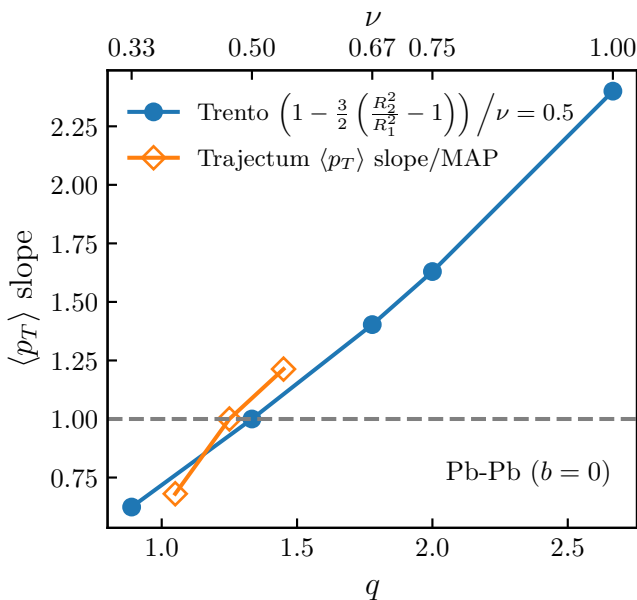


FIG. 6. Slope defined by Eq. (23), scaled by the default value c_s^2 . Orange squares: Numerical results using the *Trajectum* framework [24] as a function of the exponent q in Eq. (6). Blue circles: Our perturbative result (22) as a function of the exponent ν in Eq. (5). We assume for simplicity that q and ν are related through Eq. (7).

The first line of Eq. (23) also rules the increase of $\langle p_T \rangle$ as a function of collision energy at fixed centrality. By comparing Pb+Pb results at $\sqrt{s_{NN}} = 2.76$ TeV and 5.02 TeV, it has been shown that the value $c_s^2(T_{\text{eff}})$ inferred from this relation is compatible with that calculated in lattice QCD [18]. Note that the largest source of uncertainty in this determination is, again, the variation of the volume, but the resulting uncertainty is small.

Therefore, as the validity of thermodynamic relations and the hot QCD equation of state seems well understood, one could indeed use the increase of $\langle p_T \rangle$ in ultracentral collisions to place quantitative bounds on the relative difference between R_2^2 and R_1^2 . This provides new, non-trivial information on the distribution of entropy density fluctuations across the transverse plane.

VII. CONCLUSIONS

We have shown that the variation of the size of the quark-gluon plasma in ultracentral collisions depends on how the excess density is distributed in the transverse plane. The statistics of energy fluctuations at the time when the two nuclei interact is modified through a non-linear evolution by the pre-equilibrium dynamics, and leads to a scaling of the initial entropy density of the type $\sqrt{t_A t_B}$, making the total entropy proportional to the mass number of the colliding ions in the ultra-central

limit ($t_A = t_B$), which is well motivated by experimental results. Our main finding is that, if the multiplicity is proportional to the number of nucleons, then the excess entropy density is distributed in the same way as the average density in the transverse plane.

This leave little room for a variation of the volume with the multiplicity. However, as measurements of $\langle p_T \rangle$ in ultra-central collisions are extremely precise, it should be feasible to make precise statements in this regard based on existing data. It would be important, in particular, to repeat this analysis in ultra-central light-ion collisions [70–72]. Although highly consistent with hydrodynamic expectations, in such systems pre-equilibrium corrections are expected to play a more important role (especially at RHIC energies [73]), potentially modifying the statistics of fluctuations of the entropy density field.

We emphasize that verifying the scaling of the entropy density with the nuclear mass numbers through such measurements can have important consequences for the study of nuclear structure at colliders [74–76]. If the entropy density is such that $s(\mathbf{x}) \propto t(\mathbf{x})$ in the ultracentral limit, this implies that the collision process itself does not generate any new spatial correlations in the transverse plane [9]. Therefore, if the increase of $\langle p_T \rangle$ in ultracentral collisions confirms that the volume of the quark-gluon plasma does not increase or decrease as a function of the multiplicity, it will strengthen the argument that fluctuations in ultracentral collisions are essentially those coming from one nucleus alone. This in turn entails a straightforward relation between multiparticle correlation observables in symmetric heavy-ion collisions and many-body correlations in the ground state of the nucleus [11], as illustrated in Appendix A for two-body correlations. This will allow high-energy colliders to probe many-body properties of nuclear ground states in unprecedented detail.

ACKNOWLEDGMENTS

We thank Jean-Paul Blaizot and Aleksas Mazeliauskas for numerous discussions. F.Z. acknowledges support by the DFG through Emmy Noether Programme (project number 496831614) and CRC 1225 ISOQUANT (project number 27381115) as well as the state of Baden-Württemberg through bwHPC.

Appendix A: Why $s \propto \sqrt{t_A t_B}$ is special

In this Appendix, we derive approximate analytic expressions of density correlations in the TRENTo model for Pb+Pb collisions at $b = 0$. This specific case is simpler for two reasons:

- Target and projectile play symmetric roles at each point \mathbf{x} .

- Almost all the nucleons (98% on average in Monte Carlo Glauber calculations) participate in the collision. We make the approximation that *all* nucleons participate, which is the case at asymptotically high energies.

We start from the expression of the entropy density, Eq. (5), in which we carry out a standard fluctuation decomposition:

$$t_{A,B}(\mathbf{x}) = \langle t_A(\mathbf{x}) \rangle + \delta t_{A,B}(\mathbf{x}), \quad (\text{A1})$$

where local symmetry between target and projectile implies $\langle t_A(\mathbf{x}) \rangle = \langle t_B(\mathbf{x}) \rangle$. Inserting in Eq. (5), where we omit the global multiplicative constant, and linearizing in the fluctuations, one obtains

$$\begin{aligned} \kappa_1(\mathbf{x}) &= \langle t_A(\mathbf{x}) \rangle^{2\nu} \\ \delta s(\mathbf{x}) &= \nu \langle t_A(\mathbf{x}) \rangle^{2\nu-1} (\delta t_A(\mathbf{x}) + \delta t_B(\mathbf{x})). \end{aligned} \quad (\text{A2})$$

One immediately sees why $\nu = \frac{1}{2}$ is special, as these expressions simplify to:

$$\begin{aligned} \kappa_1(\mathbf{x}) &= \langle t_A(\mathbf{x}) \rangle \\ \delta s(\mathbf{x}) &= \frac{1}{2} (\delta t_A(\mathbf{x}) + \delta t_B(\mathbf{x})). \end{aligned} \quad (\text{A3})$$

These equations show that both the mean value and the fluctuation are linear in the thickness function for this specific choice of ν . We assume $\nu = \frac{1}{2}$ from now on.

The two point-function $\langle \delta s(\mathbf{x}) \delta s(\mathbf{y}) \rangle$, which will be needed in order to evaluate $\kappa_2(\mathbf{x})$, contains four terms. Since the two nuclei are independent, the cross correlation vanishes: $\langle \delta t_A(\mathbf{x}) \delta t_B(\mathbf{y}) \rangle = 0$. This simplification arises because we have assumed that all the nucleons are participants. Otherwise, the condition that a nucleon participates induces correlations between the two colliding nuclei, which are dubbed “twin correlations” [77]. The only nonvanishing terms are $\langle \delta t_A(\mathbf{x}) \delta t_A(\mathbf{y}) \rangle$ and $\langle \delta t_B(\mathbf{x}) \delta t_B(\mathbf{y}) \rangle$ which are equal by symmetry. We thus obtain:

$$\langle \delta s(\mathbf{x}) \delta s(\mathbf{y}) \rangle = \frac{1}{2} \langle \delta t_A(\mathbf{x}) \delta t_A(\mathbf{y}) \rangle. \quad (\text{A4})$$

This equation shows that the two-point correlation of the entropy density profile is simply related to that of a single nucleus [11].

We have related the statistical properties of the entropy density to those of the thickness function $t_A(\mathbf{x})$. In order to evaluate them, we go back to the definition [26]:

$$t_A(\mathbf{x}) = \sum_{i=1}^A w_i \rho_p(\mathbf{x} - \mathbf{x}_i), \quad (\text{A5})$$

where the sum runs over all nucleons, $A = 208$ for Pb, and

- w_i are independent weights sampled according to a gamma distribution, which satisfies

$$\begin{aligned} \langle w \rangle &= 1 \\ \langle w^2 \rangle &= 1 + \frac{1}{k}. \end{aligned} \quad (\text{A6})$$

- \mathbf{x}_i is the transverse position of nucleon i ,
- $\rho_p(\mathbf{x})$ is the normalized “nucleon profile”.

We make the approximation that the nucleon size is much smaller than the nuclear radius, and treat the profile as a Dirac peak: $\rho_p(\mathbf{x}) \approx \delta(\mathbf{x})$. The effect of the nucleon size is discussed in Appendix B.

We now evaluate the one- and two-point functions of $t_A(\mathbf{x})$. The probability distribution of \mathbf{x}_i is $T_A(\mathbf{x}_i)/A$, where $T_A(\mathbf{x})$ denotes the usual thickness function of the nucleus in an optical Glauber calculation [54], that is, the integral of the nucleon density over the longitudinal coordinate. Since there are A identical terms, the mean value of $t_A(\mathbf{x})$ is:

$$\kappa_1(\mathbf{x}) = \langle t_A(\mathbf{x}) \rangle = \int_{\mathbf{y}} T_A(\mathbf{y}) \delta(\mathbf{x} - \mathbf{y}) = T_A(\mathbf{x}), \quad (\text{A7})$$

where we have used $\langle w_i \rangle = 1$.

We now evaluate the two-point function. Eq. (A5) gives

$$t_A(\mathbf{x}) t_A(\mathbf{y}) = \sum_{i=1}^A \sum_{j=1}^A w_i w_j \delta(\mathbf{x} - \mathbf{x}_i) \delta(\mathbf{y} - \mathbf{x}_j). \quad (\text{A8})$$

There are A^2 terms, which consist of $A(A-1)$ non-diagonal terms with $i \neq j$ and A diagonal terms. Since the nucleons are sampled independently, \mathbf{x}_i and \mathbf{x}_j are independent for $i \neq j$ (unless an excluded volume is implemented in the Glauber calculation [78]). We average over events, separating the diagonal and non-diagonal terms, and using Eqs. (A6):

$$\begin{aligned} \langle t_A(\mathbf{x}) t_A(\mathbf{y}) \rangle &= \left(1 + \frac{1}{k}\right) T_A(\mathbf{x}) \delta(\mathbf{x} - \mathbf{y}) \\ &\quad + \left(1 - \frac{1}{A}\right) T_A(\mathbf{x}) T_A(\mathbf{y}). \end{aligned} \quad (\text{A9})$$

Using Eqs. (A1), (A7) and (A9), we obtain the following expression of the density-density correlation (A4):

$$\begin{aligned} \langle \delta s(\mathbf{x}) \delta s(\mathbf{y}) \rangle &= \frac{1}{2} (\langle t_A(\mathbf{x}) t_A(\mathbf{y}) \rangle - \langle t_A(\mathbf{x}) \rangle \langle t_A(\mathbf{y}) \rangle) \\ &= \frac{1}{2} \left(1 + \frac{1}{k}\right) T_A(\mathbf{x}) \delta(\mathbf{x} - \mathbf{y}) \\ &\quad - \frac{1}{2A} T_A(\mathbf{x}) T_A(\mathbf{y}). \end{aligned} \quad (\text{A10})$$

It consists of a positive short-range part, $\delta(\mathbf{x} - \mathbf{y})$, and a negative long-range part induced by the condition that the total number of nucleons is fixed. In the case $\nu = 1$, a similar negative long-range correlation is present, whose analytic expression could easily be obtained in the same way. It explains the negative values of $\kappa_2(r)$ observed in the bottom panel of Fig. 4 and discussed in Sec. V.

We finally integrate Eq. (A10) over \mathbf{y} to obtain $\kappa_2(\mathbf{x})$, defined by Eq. (14):

$$\kappa_2(\mathbf{x}) = \int_{\mathbf{y}} \langle \delta s(\mathbf{x}) \delta s(\mathbf{y}) \rangle = \frac{1}{2k} T_A(\mathbf{x}), \quad (\text{A11})$$

where we have used $\int_{\mathbf{y}} T_A(\mathbf{y}) = A$. Comparing with Eq. (A7), one sees that $\kappa_2(\mathbf{x})$ and $\kappa_1(\mathbf{x})$ are proportional to one another, as observed in Fig. 4. According to Eq. (16), this means that excess density in ultracentral collision is distributed in the same way as the mean density. This explains why the radius is independent of the size, as observed in Fig. 3 for $\nu = 0.5$.

As a byproduct of this calculation, we finally derive an analytic expression of the variance of the total entropy. Using Eqs. (10), (15), (A7) and (A11), one obtains

$$\frac{\sigma_S^2}{S_{\text{knee}}^2} = \frac{\int_{\mathbf{x}} \kappa_2(\mathbf{x})}{\left(\int_{\mathbf{x}} \kappa_1(\mathbf{x})\right)^2} = \frac{1}{2kA}. \quad (\text{A12})$$

The value of k that satisfies the constraint from ATLAS data, Eq. (8), is $k \approx 1.2$, in reasonable agreement with the value $k = 1.4$ reported in Fig. 1. This equation also shows that the gamma fluctuations implemented in the TRENTo model via the parameter k are solely responsible for the fluctuations of the total entropy for $\nu = 0.5$. In the limit $k \rightarrow \infty$, the weights w_j in Eq. (A5) are all equal to unity, and the only remaining fluctuations are those of the positions of nucleons. In this limit, entropy fluctuations vanish, which means that fluctuations in nucleon positions do not contribute to entropy fluctuations to leading order. It is quite a remarkable result, as these fluctuations produce sizable fluctuations in other observables, such as initial anisotropies [79, 80].

Appendix B: Influence of the nucleon width

In the TRENTo model, the nucleon width w_p enters the profile function associated with each participant in (A5), which is modeled as a Gaussian [26]:

$$\rho_p(x) = \frac{1}{2\pi w_p^2} \exp\left(-\frac{x^2}{2w_p^2}\right), \quad (\text{B1})$$

Within the approximations made in Appendix A, w_p does not enter any of our results. In this Appendix, we illustrate the effect of the nucleon width by evaluating more precisely the average density profile $\kappa_1(\mathbf{x})$, taking into account terms of order 2 in the fluctuations, which have been neglected so far.

Using Eq. (A1), we obtain

$$\begin{aligned} t_A(\mathbf{x})^{1/2} &= (T_A(\mathbf{x}) + \delta t_A(\mathbf{x}))^{1/2} \\ &= T_A(\mathbf{x})^{1/2} \left(1 + \frac{1}{2} \frac{\delta t_A(\mathbf{x})}{T_A(\mathbf{x})} - \frac{1}{8} \frac{\delta t_A(\mathbf{x})^2}{T_A(\mathbf{x})^2}\right). \end{aligned} \quad (\text{B2})$$

Carrying out a similar decomposition of $t_B(\mathbf{x})$, inserting into Eq. (5) with $\nu = \frac{1}{2}$, and averaging over events, we obtain the following expression of the mean entropy density:

$$\kappa_1(\mathbf{x}) = \langle t_A(\mathbf{x}) \rangle - \frac{1}{4} \frac{\langle \delta t_A(\mathbf{x})^2 \rangle}{T_A(\mathbf{x})}, \quad (\text{B3})$$

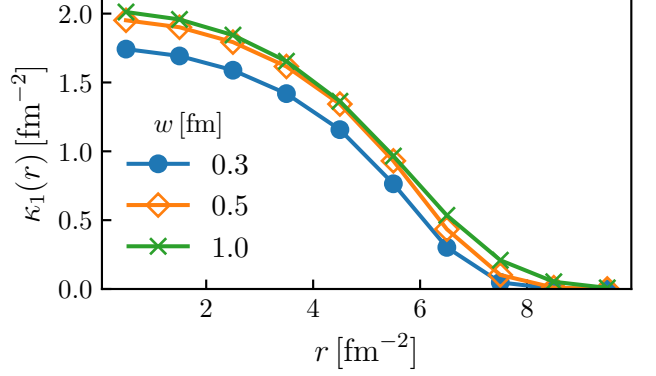


FIG. 7. Dependence of the average entropy density $\kappa_1(r)$ on the nucleon radius in the TRENTo model. The entropy density is defined by Eq. (5), where $\nu = \frac{1}{2}$ and the proportionality factor has been set to unity. The thickness functions $t_{A,B}(\mathbf{x})$ are defined by Eq. (A5). Results for Pb+Pb collisions at $b = 0$ are displayed for three different values of the nucleon width w_p .

where we have used the independence between the fluctuations in the two nuclei $\langle \delta t_A(\mathbf{x}) \delta t_B(\mathbf{x}) \rangle = 0$. The correction induced by fluctuations is proportional to the variance of the local density, $\langle \delta t_A(\mathbf{x})^2 \rangle$.

This variance is evaluated using Eq. (A8), in which we set $\mathbf{y} = \mathbf{x}$, and where we replace the Dirac peaks by the actual density profile $\rho_p(\mathbf{x})$ of the nucleon. The dominant contribution comes from the diagonal terms with $i = j$ and one obtains, after averaging over events:

$$\begin{aligned} \langle \delta t_A(\mathbf{x})^2 \rangle &= \langle w_i^2 \rangle T_A(\mathbf{x}) \int_{\mathbf{z}} \rho_p(\mathbf{z})^2 \\ &= \left(1 + \frac{1}{k}\right) T_A(\mathbf{x}) \frac{1}{8\pi w_p^2}, \end{aligned} \quad (\text{B4})$$

where, in the last equality, we have used Eqs. (A6) and (B1). Inserting into Eq. (B3), and using (A7), we finally obtain:

$$\kappa_1(x) = T_A(x) - \frac{1 + \frac{1}{k}}{16\pi w_p^2}. \quad (\text{B5})$$

The net effect of fluctuations is that they shift the mean entropy density by a negative additive constant. [Note that the mean entropy density must be negative, so that the validity of Eq. (B5) breaks down for large r .] This shift is inversely proportional to w_p^2 , which can be understood as follows: A smaller nucleon has a smaller probability of colliding with other nucleons, leading to a decrease in the density. Fig. 7 displays numerical results for three different values of w_p . Eq. (B5) predicts that $\kappa_1(r)$ is smaller by 0.1 fm^{-2} for $w_p = 0.5 \text{ fm}$ than for $w_p = 1 \text{ fm}$, and by 0.24 fm^{-2} for $w_p = 0.3 \text{ fm}$ than for $w_p = 0.5 \text{ fm}$, in fair agreement with the numerical results.

[1] S. Chatrchyan *et al.* [CMS], JHEP **02**, 088 (2014) [arXiv:1312.1845 [nucl-ex]].

[2] M. Luzum and J. Y. Ollitrault, Nucl. Phys. A **904-905**, 377c-380c (2013) [arXiv:1210.6010 [nucl-th]].

[3] C. Shen, Z. Qiu and U. Heinz, Phys. Rev. C **92**, no.1, 014901 (2015) [arXiv:1502.04636 [nucl-th]].

[4] S. J. Das, G. Giacalone, P. A. Monard and J. Y. Ollitrault, Phys. Rev. C **97**, no.1, 014905 (2018) [arXiv:1708.00081 [nucl-th]].

[5] R. Samanta, S. Bhatta, J. Jia, M. Luzum and J. Y. Ollitrault, Phys. Rev. C **109**, no.5, L051902 (2024) [arXiv:2303.15323 [nucl-th]].

[6] L. M. Liu, C. J. Zhang, J. Zhou, J. Xu, J. Jia and G. X. Peng, Phys. Lett. B **834**, 137441 (2022) [arXiv:2203.09924 [nucl-th]].

[7] H. Zhang, A. Akridge, C. J. Horowitz, J. Liao and H. Xing, [arXiv:2510.07816 [nucl-th]].

[8] J. P. Blaizot, W. Broniowski and J. Y. Ollitrault, Phys. Lett. B **738**, 166-171 (2014) [arXiv:1405.3572 [nucl-th]].

[9] G. Giacalone, Eur. Phys. J. A **59**, no.12, 297 (2023) [arXiv:2305.19843 [nucl-th]].

[10] H. Mehrabpour, [arXiv:2506.12673 [nucl-th]].

[11] T. Duguet, G. Giacalone, S. Jeon and A. Tichai, Phys. Rev. Lett. **135**, no.18, 182301 (2025) [arXiv:2504.02481 [nucl-th]].

[12] Q. Liu, H. Mehrabpour and B. N. Lu, [arXiv:2509.00315 [nucl-th]].

[13] K. V. Yousefnia, A. Kotibhaskar, R. Bhalerao and J. Y. Ollitrault, Phys. Rev. C **105**, no.1, 014907 (2022) [arXiv:2108.03471 [nucl-th]].

[14] M. Pepin, P. Christiansen, S. Munier and J. Y. Ollitrault, Phys. Rev. C **107**, no.2, 024902 (2023) [arXiv:2208.12175 [nucl-th]].

[15] A. Hayrapetyan *et al.* [CMS], Rept. Prog. Phys. **87**, no.7, 077801 (2024) [arXiv:2401.06896 [nucl-ex]].

[16] G. Aad *et al.* [ATLAS], Phys. Rev. Lett. **133**, no.25, 252301 (2024) [arXiv:2407.06413 [nucl-ex]].

[17] I. J. Abualrob *et al.* [ALICE], [arXiv:2506.10394 [nucl-ex]].

[18] F. G. Gardim, G. Giacalone, M. Luzum and J. Y. Ollitrault, Nature Phys. **16**, no.6, 615-619 (2020) [arXiv:1908.09728 [nucl-th]].

[19] F. G. Gardim, G. Giacalone and J. Y. Ollitrault, Phys. Lett. B **809**, 135749 (2020) [arXiv:1909.11609 [nucl-th]].

[20] F. G. Gardim, A. V. Giannini and J. Y. Ollitrault, Phys. Lett. B **856**, 138937 (2024) [arXiv:2403.06052 [nucl-th]].

[21] G. Soares Rocha, L. Gavassino, M. Singh and J. F. Paquet, Phys. Rev. C **110**, no.3, 034913 (2024) [arXiv:2405.10401 [hep-ph]].

[22] J. A. Sun and L. Yan, Phys. Lett. B **866**, 139507 (2025) [arXiv:2407.05570 [nucl-th]].

[23] Y. S. Mu, J. A. Sun, L. Yan and X. G. Huang, Phys. Rev. Lett. **135**, no.16, 162301 (2025) [arXiv:2501.02777 [nucl-th]].

[24] G. Nijs and W. van der Schee, Phys. Lett. B **853**, 138636 (2024) [arXiv:2312.04623 [nucl-th]].

[25] L. Gavassino, H. Hirvonen, J. F. Paquet, M. Singh and G. Soares Rocha, [arXiv:2503.20765 [hep-ph]].

[26] J. S. Moreland, J. E. Bernhard and S. A. Bass, Phys. Rev. C **92**, no.1, 011901 (2015) [arXiv:1412.4708 [nucl-th]].

[27] G. Nijs and W. van der Schee, [arXiv:2304.06191 [nucl-th]].

[28] J. D. Bjorken, Phys. Rev. D **27**, 140-151 (1983)

[29] S. Eremin and S. Voloshin, Phys. Rev. C **67**, 064905 (2003) [arXiv:nucl-th/0302071 [nucl-th]].

[30] L. Adamczyk *et al.* [STAR], Phys. Rev. Lett. **115**, no.22, 222301 (2015) [arXiv:1505.07812 [nucl-ex]].

[31] J. E. Bernhard, J. S. Moreland, S. A. Bass, J. Liu and U. Heinz, Phys. Rev. C **94**, no.2, 024907 (2016) [arXiv:1605.03954 [nucl-th]].

[32] D. Everett *et al.* [JETSCAPE], Phys. Rev. C **103**, no.5, 054904 (2021) [arXiv:2011.01430 [hep-ph]].

[33] G. Nijs, W. van der Schee, U. Gürsoy and R. Snellings, Phys. Rev. Lett. **126**, no.20, 202301 (2021) [arXiv:2010.15130 [nucl-th]].

[34] G. Nijs, W. van der Schee, U. Gürsoy and R. Snellings, Phys. Rev. C **103**, no.5, 054909 (2021) [arXiv:2010.15134 [nucl-th]].

[35] J. E. Parkkila, A. Onnerstad, S. F. Taghavi, C. Mordasini, A. Bilandzic, M. Virta and D. J. Kim, Phys. Lett. B **835**, 137485 (2022) [arXiv:2111.08145 [hep-ph]].

[36] D. Liyanage, Ö. Sürer, M. Plumlee, S. M. Wild and U. Heinz, Phys. Rev. C **108**, no.5, 054905 (2023) [arXiv:2302.14184 [nucl-th]].

[37] G. Giacalone, G. Nijs and W. van der Schee, Phys. Rev. Lett. **131**, no.20, 20 (2023) [arXiv:2305.00015 [nucl-th]].

[38] M. Virta, J. Parkkila and D. J. Kim, Phys. Rev. C **111**, no.4, 044903 (2025) [arXiv:2411.01932 [hep-ph]].

[39] S. Jaiswal, [arXiv:2509.19759 [hep-ph]].

[40] K. J. Eskola, K. Kajantie, P. V. Ruuskanen and K. Tuominen, Nucl. Phys. B **570**, 379-389 (2000) [arXiv:hep-ph/9909456 [hep-ph]].

[41] K. J. Eskola, P. V. Ruuskanen, S. S. Rasanen and K. Tuominen, Nucl. Phys. A **696**, 715-728 (2001) [arXiv:hep-ph/0104010 [hep-ph]].

[42] O. Garcia-Montero and S. Schlichting, Eur. Phys. J. A **61** (2025) no.3, 54 doi:10.1140/epja/s10050-025-01523-7 [arXiv:2502.09721 [hep-ph]].

[43] T. Lappi and L. McLerran, Nucl. Phys. A **772**, 200-212 (2006) [arXiv:hep-ph/0602189 [hep-ph]].

[44] X. Artru and G. Mennessier, Nucl. Phys. B **70**, 93-115 (1974)

[45] B. Andersson, G. Gustafson, G. Ingelman and T. Sjstrand, Phys. Rept. **97**, 31-145 (1983)

[46] T. Lappi, Phys. Lett. B **643**, 11-16 (2006) [arXiv:hep-ph/0606207 [hep-ph]].

[47] J. Berges, M. P. Heller, A. Mazeliauskas and R. Venugopalan, Rev. Mod. Phys. **93**, no.3, 035003 (2021) [arXiv:2005.12299 [hep-th]].

[48] J. Jankowski, S. Kamata, M. Martinez and M. Spaliński, Phys. Rev. D **104**, no.7, 074012 (2021) [arXiv:2012.02184 [nucl-th]].

[49] J. P. Blaizot and L. Yan, Annals Phys. **412**, 167993 (2020) [arXiv:1904.08677 [nucl-th]].

[50] N. Borghini, M. Borrell, N. Feld, H. Roch, S. Schlichting and C. Werthmann, Phys. Rev. C **107**, no.3, 034905 (2023) [arXiv:2209.01176 [hep-ph]].

[51] W. Busza, K. Rajagopal and W. van der Schee, Ann. Rev. Nucl. Part. Sci. **68**, 339-376 (2018) [arXiv:1802.04801 [hep-ph]].

[52] G. Giacalone, A. Mazeliauskas and S. Schlichting, Phys. Rev. Lett. **123**, no.26, 262301 (2019) [arXiv:1908.02866

[hep-ph]].

[53] J. Y. Ollitrault, Eur. J. Phys. **29**, 275-302 (2008) [arXiv:0708.2433 [nucl-th]].

[54] M. L. Miller, K. Reygers, S. J. Sanders and P. Steinberg, Ann. Rev. Nucl. Part. Sci. **57**, 205-243 (2007) [arXiv:nucl-ex/0701025 [nucl-ex]].

[55] C. Loizides, J. Nagle and P. Steinberg, SoftwareX **1-2**, 13-18 (2015) [arXiv:1408.2549 [nucl-ex]].

[56] J. S. Moreland, J. E. Bernhard and S. A. Bass, Phys. Rev. C **101**, no.2, 024911 (2020) [arXiv:1808.02106 [nucl-th]].

[57] A. Kirchner and S. A. Bass, [arXiv:2508.20390 [hep-ph]].

[58] G. Nijs and W. van der Schee, Phys. Rev. Lett. **129**, no.23, 232301 (2022) [arXiv:2206.13522 [nucl-th]].

[59] G. Giacalone, [arXiv:2208.06839 [nucl-th]].

[60] P. Carzon, M. D. Sievert and J. Noronha-Hostler, Phys. Rev. C **105**, no.1, 014913 (2022) [arXiv:2106.02525 [nucl-th]].

[61] J. E. Bernhard, J. S. Moreland and S. A. Bass, Nature Phys. **15**, no.11, 1113-1117 (2019)

[62] P. Hanus, A. Mazeliauskas and K. Reygers, Phys. Rev. C **100**, no.6, 064903 (2019) [arXiv:1908.02792 [hep-ph]].

[63] P. Bozek and W. Broniowski, Phys. Rev. C **85**, 044910 (2012) [arXiv:1203.1810 [nucl-th]].

[64] S. A. Voloshin, A. M. Poskanzer, A. Tang and G. Wang, Phys. Lett. B **659**, 537-541 (2008) [arXiv:0708.0800 [nucl-th]].

[65] A. Bzdak and V. Koch, Phys. Rev. C **86**, 044904 (2012) [arXiv:1206.4286 [nucl-th]].

[66] L. Adamczyk *et al.* [STAR], Phys. Rev. Lett. **112**, 032302 (2014) [arXiv:1309.5681 [nucl-ex]].

[67] R. Rogly, G. Giacalone and J. Y. Ollitrault, Phys. Rev. C **99**, no.3, 034902 (2019) [arXiv:1809.00648 [nucl-th]].

[68] P. Braun-Munzinger, K. Redlich, A. Rustamov and J. Stachel, JHEP **08**, 113 (2024) [arXiv:2312.15534 [nucl-th]].

[69] E. Roubertie, M. Verdan, A. Kirchner and J. Y. Ollitrault, Phys. Rev. C **111**, no.6, 064906 (2025) [arXiv:2503.17035 [nucl-th]].

[70] G. Aad *et al.* [ATLAS], [arXiv:2509.05171 [nucl-ex]].

[71] I. J. Abualrob *et al.* [ALICE], [arXiv:2509.06428 [nucl-ex]].

[72] A. Hayrapetyan *et al.* [CMS], [arXiv:2510.02580 [nucl-ex]].

[73] [STAR], [arXiv:2510.19645 [nucl-ex]].

[74] J. Jia, G. Giacalone, B. Bally, J. D. Brandenburg, U. Heinz, S. Huang, D. Lee, Y. J. Lee, C. Loizides and W. Li, *et al.* Nucl. Sci. Tech. **35**, no.12, 220 (2024) [arXiv:2209.11042 [nucl-ex]].

[75] M. I. Abdulhamid *et al.* [STAR], Nature **635**, no.8037, 67-72 (2024) [arXiv:2401.06625 [nucl-ex]].

[76] G. Giacalone, J. Jia, V. Somà, Y. Zhou, A. Afanasejev, M. Alvioli, B. Bally, F. Capellino, J. P. Ebran and H. Elfner, *et al.* [arXiv:2507.01454 [nucl-ex]].

[77] J. P. Blaizot, W. Broniowski and J. Y. Ollitrault, Phys. Rev. C **90**, no.3, 034906 (2014) [arXiv:1405.3274 [nucl-th]].

[78] M. Luzum, M. Hippert and J. Y. Ollitrault, Eur. Phys. J. A **59**, no.5, 110 (2023) [arXiv:2302.14026 [nucl-th]].

[79] B. Alver *et al.* [PHOBOS], Phys. Rev. Lett. **98**, 242302 (2007) [arXiv:nucl-ex/0610037 [nucl-ex]].

[80] B. Alver and G. Roland, Phys. Rev. C **81**, 054905 (2010) [erratum: Phys. Rev. C **82**, 039903 (2010)] [arXiv:1003.0194 [nucl-th]].